J. Am. Soc. Mass Spectrom. (2015) 26:1665–1675
DOI: 10.1007/s13361-015-1199-6

RESEARCH ARTICLE

Insights on Clusters Formation Mechanism by Time of Flight Mass Spectrometry. 1. The Case of Ethanol–Water Clusters

Xinling Li,[1,2] Xuan Wang,[3] Maria dell'Arco Passaro,[1,4] Nicola Spinelli,[5] Barbara Apicella[1]

[1]Istituto di Ricerche sulla Combustione, IRC–CNR, P.le Tecchio 80, 80125, Napoli, Italy
[2]Key Laboratory of Power Machinery and Engineering, Ministry of Education, Shanghai Jiao Tong University, Shanghai, 200240, China
[3]SPIN - CNR, Via Cintia, 80124, Napoli, Italy
[4]Chemical Engineering, Materials and Industrial Production Department, University of Naples Federico II, P.le Tecchio 80, 80125, Napoli, Italy
[5]CNISM and Physics Department, University of Naples Federico II, Via Cintia, 80124, Napoli, Italy

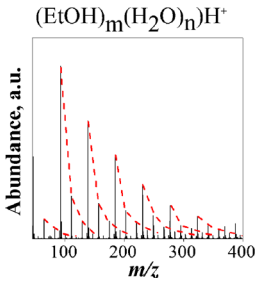

Abstract. In the present work, water clusters with the addition of an electrophilic molecule such as ethanol have been studied by time of flight mass spectrometry (TOFMS). Mass distributions of molecular clusters of ethanol, water, and ethanol–water mixed clusters were obtained by two different ionization methods: electron ionization (EI) and picosecond laser photo-ionization (PI) at a wavelength of 355 nm. It was shown that short pulse laser ionization increases the signal intensity and promotes the extension of the detected mass range of the clusters in comparison with EI. Much larger clusters were detected in our experiments with respect to the current literature. The autocorrelation function (AF) was introduced in the analysis of the composition of the water clusters in terms of fundamental periodicities for obtaining information on clusters formation mechanisms. Besides, it was found that ethanol molecules are capable of substitutional interaction with hydrogen-bonded water clusters in ethanol–water binary mixtures but the self-association of ethanol was the dominant process. Moreover, the increase of ethanol concentration promotes both the formation of hydrated ethanol clusters and the self-association of ethanol clusters in ethanol–water binary mixtures. The formation of water-rich clusters and subsequent metastable fragmentation were found to be the dominant processes determining the water-rich cluster distribution, irrespective of the ionization process, while the ionization process significantly affects the ethanol-rich cluster distribution.

Keywords: Reflectron time-of-flight mass spectrometry, Short-pulse laser, Photo-ionization, Ethanol–water clusters

Received: 9 April 2015/Revised: 18 May 2015/Accepted: 18 May 2015/Published Online: 23 July 2015

Introduction

Molecular clusters of different sizes starting from small molecules, such as water molecules, can be easily formed in a supersonic free jet expansion [1–3]. Many papers have been published on water clusters, mainly aiming for the possibility of using them as a vehicle for systematically studying molecular properties of water [4–9]. Nevertheless, not all is known about the different-size water clusters formation and ionization.

In the present work, water clusters were produced in a supersonic expansion and studied by a reflectron time of flight mass spectrometer (*r*-TOFMS) using an electron beam and a laser beam as ionization sources. In order to deep the information of cluster formation, two kinds of additives were added to water clusters: ethanol and acetone. Both additives have proton affinities higher with respect to water (acetone more than ethanol) and thus change the cluster network. Indeed, when a solvent molecule is replaced by another molecule with larger proton affinity, the strength of all other hydrogen bonds decreases, on the basis of the concept of "anticooperativity" by successive substitutions in a mixed solvation system

Electronic supplementary material The online version of this article (doi:10.1007/s13361-015-1199-6) contains supplementary material, which is available to authorized users.

Correspondence to: Barbara Apicella; *e-mail:* apicella@irc.cnr.it

introduced by Bing et al. [10]. However, ethanol and acetone present a very different hydrogen-bonding ability: ethanol molecules have both H-bond acceptor and donor sites, whereas acetone molecules have only acceptor sites (two lone pairs). This difference enables different water–water/water–additive/additive–additive interactions, the study of which will allow going deep into the mechanisms of cluster formation.

The results obtained with ethanol are reported in the present paper, whereas the results on acetone along with the comparison with ethanol–water mixed clusters are reported in a paper in preparation [Li, X., Passaro M., Apicella, B.: *Insights on clusters formation mechanism by time of flight mass spectrometry. 2. The case of acetone–water clusters.*].

Moreover, relatively simple alcohol–water mixtures, as well as ethanol–water mixtures, constitute interesting systems to be investigated also because they are frequently used as solvents in studies of chemical equilibria and reactions as well as in various biological studies, and they may serve as models helpful for a better understanding of more complex systems [11].

Small alcohols such as methanol and ethanol are miscible with water at any mixing ratio, while surface tension measurements about the ethanol–water binary mixture show that the surface tension decreases sharply as the ethanol mole fraction in the liquid reaches ~0.25 [12], indicating that the molecular structure of the ethanol–water solution may be different from that of pure water.

A large number of experimental studies [13–22] and simulation studies [23] have been carried out in alcohol–water mixtures. Li et al. [17] measured the surface concentration in the ethanol–water system by employing neutron reflection and found that the thickness and position of the ethanol layer suggests that molecules may be partially oriented with the ethyl group pointing towards the vapor phase.

The so-called microscopic phase separation for ethanol–water binary mixtures was presented by Egashira and Nishi [16], based on a Raman spectroscopy experiment. They found that ethanol–water binary solutions do not get ideally mixed on the molecular level as they form water cluster units and ethanol cluster units with hydrogen bonds between them constituting a sort of double-layer sandwich cluster. This structure is thought to be a moving unit in the binary solution; therefore, it must be somewhat fragile.

Other optical spectroscopic methods, such as X-ray diffraction [13] and infrared spectroscopy [24], were also used in the clusters of alcohol–water binary mixture state analysis. Although the optical spectroscopic methods are useful for investigating the structure of isolated clusters, they do not provide information about the size distribution of clusters unless coupled with mass spectrometric systems [10, 25].

The cluster size distribution is an important factor to understand the microscopic structures of liquids as well as chemical reactions in solutions. Mass spectrometry, which can precisely obtain information about the cluster size distribution, was widely used in ethanol–water mixture studies. Clusters in gas and condensed phases for mass spectrometric analysis were generated by several techniques. The supersonic expansion is one of the prominent methods to generate clusters, which are produced in vacuum by an expansion of sample vapor mixed with inert gas at high pressure through a nozzle [22, 26]. Another method is the adiabatic expansion of a liquid jet, in which a liquid sample is directly fed to a vacuum system through an injector nozzle; in this case, the droplets explode adiabatically into high vacuum [14, 15, 20, 21] and the clusters produced during the injection are ionized by electron ionization (EI) or photo-ionization (PI). Nishi et al. [14, 15] carried out ethanol–water mixture solution cluster studies by mass spectrometry with EI. They found that in the region of ethanol mole fraction (x_E) < 0.04, the mass spectrometric signals generated from ethanol monomers and "oligomers" [i.e., ethanol clusters with generic formula $(C_2H_5OH)_mH^+$] are followed by long water sequences of hydrated species $(C_2H_5OH)_m(H_2O)_nH^+$. At low temperatures, the hydrogen bond formation between two ethanol molecules becomes predominant and water molecules tend to participate in hydrophobic hydration of the ethyl groups of the oligomeric structures. This water shell was not seen for the mixtures with x_E > 0.04. It was suggested that hydrophobic hydration of ethanol is so strong that pure water clusters are not detectable as ethanol molar fraction concentration is over 0.04 [17]. At x_E = 0.08, the growth of ethanol "oligomers" is almost saturated. In ethanol-rich solutions (x_E > 0.5), the intensity of the "oligomers" becomes weaker with decreasing water content. Neat ethanol did not produce large oligomers any more.

Wakisaka and Matsuura [20], and Wakisaka and Ohki [21] have also done a series of ethanol–water studies based on mass spectrometry. They showed that ethanol-rich clusters and water-rich clusters coexist in ethanol–water binary mixtures, exhibiting microscopic phase separation at the cluster level in wide mixing ratios: 10 vol.% < [EtOH] < 90 vol.%. The self-association of alcohol molecules complements the loss of stabilization energy caused by the relatively weak coexisting interactions among different clusters. This "complementary relationship" among intermolecular interactions is an inherent property of solutions, and plays a key role in the phase separation process.

Some studies about the clusters of water and alcohols based on TOFMS with photo-ionization have been carried out [5, 18, 22, 26–29]. These works provide excellent information about the clusters mass spectra. For example, ion signals of large water clusters containing up to 60 monomers were observed for water clusters by using vacuum-ultraviolet photo–ionization (VUV-PI) [27]. In the meantime, metastable fragmentation characteristics have been found to be dependent on the different ionization methods.

In a very recent paper [5], it was shown that the decrease of the laser pulse width is an effective way for further reduction of fragmentation and increasing of the ionization efficiency. Indeed, by using laser ionization with ultrashort pulses (in the picosecond range), the detection of water clusters was found to be largely extended up to about 180 monomers (by using the TOFMS in linear configuration) [5].

In the present work, a short pulse picosecond laser associated with a reflectron time of flight mass spectrometer was used to study the clusters of ethanol–water binary mixture solutions. A wavelength of 355 nm was employed as in a previous work [5] and a large increase of ionization efficiency at 355 nm for pure water clusters compared with that at 266 nm was found because of the occurrence of a (3 + 1) resonance-enhanced multi-photon ionization (REMPI) process.

Much larger clusters were detected in our experiments with respect to the current literature. A comparison with EI was also reported. The autocorrelation function (AF) was used to analyze the composition of the water clusters in terms of fundamental periodicities.

More insights on water clusters formation and water–ethanol binary solution structures at cluster level were obtained from this study. It was found that ethanol added to water leads to a substitutional mechanism; that is, water molecules are progressively replaced by ethanol in the hydrogen bonded structures. The formation of water-rich clusters and their subsequent metastable fragmentation is the dominant process that determines the clusters distribution, irrespective of the ionization process, whereas the ionization process significantly affects the ethanol-rich cluster distribution.

Experimental and Methods

The vapor samples were produced at a temperature of 28°C, making a nitrogen gas flow (at a pressure of 3 bars) bubbling in a reservoir filled with a solution (pure water or water–ethanol mixture solution) at the entrance of the TOFMS. The TOFMS system has been described in detail in a previous paper [28]. Briefly, the sampled gases enter the first chamber of the instrument through a solenoid actuated valve (Parker Hannifin Corporation, General Valve Division, Fairfield, NJ, USA) equipped with a 0.8 mm aperture nozzle generating a pulsed supersonic jet. The valve was modified in order to minimize the dead volume and to increase the suction efficiency. The central part of the jet is extracted by a skimmer to produce a pulsed molecular beam, which is ionized and analyzed by a Wiley-McLaren reflectron TOFMS instrument (Kaesdorf s.r.l., Munchen, Germany) where different types of ionization sources can be used.

The TOFMS system can be operated with a mass filter to deflect the lowest mass ions by a pulsed electric field. In these conditions, the saturation of the detector (a microchannel plate-MCP) due to the very high signal intensities produced by the most abundant low-mass ions is avoided and the dynamic range of the detector is preserved. The use of the mass filter strongly reduces the signals below *m/z* 50, hindering the overloading of the detector by the most abundant and easily detectable low masses species. For this reason, in the following the mass spectra have been reported starting from this *m/z* value.

For EI, the electrons are produced by a hot tungsten loop filament and accelerated to 70 eV kinetic energy. In the present experiment, a pulse duration of 2 μs with a repetition rate of 20 Hz was used for EI, in order to use the same frequency of the laser, for a more reliable comparison between EI and photoionization.

Short pulses photoionization (PI) was also employed by using the third harmonic of a Nd:YAG pulsed laser (Leopard Series model D-20; Continuum, Santa Clara, CA, USA) with a repetition rate of 20 Hz and pulse duration of 20 ps. The maximum peak energy was 8 mJ, while the corresponding power density (*PD*) was 3.24×10^{11} W/cm^2. A focusing lens was employed and the beam spot area was approximately 1.2×10^{-3} cm^2. Special grade (>99%) ethanol was used, mixed with purified water with different volume and mole ratios. In the present paper, the ethanol volumetric ratio V_E/V_S was defined as the ratio between the liquid ethanol volume and the volume of solution and x_E as the corresponding molar ratio (ratio between ethanol mole and total moles in water/ethanol solution). The values of V_E/V_S and x_E employed are reported in Table 1.

Results and Discussions

Mass Spectrometric Analysis of Ethanol–Water Clusters

Mass spectra of pure water clusters by TOFMS both with EI and PI present regular sequences of peaks with gaps of *m/z* 18, as reported in [5].

It is known that photoionization of neutral water clusters creates unstable cations, $[(H_2O)_n]^+$, which undergo very fast intracluster charge redistribution on the subpicosecond time scale. The thermodynamically and kinetically most favorable reaction pathway is a proton transfer with subsequent OH· loss, forming protonated water clusters, $(H_2O)_nH^+$. Therefore, the protonated water clusters, besides $[(H_2O)]^+$ and $(H_2O)_2^+$, become the dominant peaks in almost all mass spectrometric studies of water clusters employing various ionization techniques [27]. Stace and Shukla [30] reported that in the case of ethanol clusters, a similar mechanism occurs and the proton remains preferentially attached on an ethanol molecule, with the elimination of OH radical.

In the experimental conditions employed in the present work, protonated cluster ions dominate the spectra of both pure water clusters, water–ethanol, and pure ethanol clusters; therefore, the following discussion will take into account only their

Table 1. Ethanol Volumetric Ratios V_E/V_S Studied in This Work and Corresponding Ethanol Mole Fractions in the Liquid Solution x_E

V_E/V_S, %	x_E, mol/mol
0	0
5	0.016
10	0.034
15	0.055
20	0.072
25	0.10
30	0.12
35	0.15
40	0.17

presence, neglecting the neutral cluster ions. The use of the mass filter strongly reduces the signals below *m/z* 50; therefore, in the following the mass spectra have been reported starting from this *m/z* value. However, in the mass range lower than *m/z* 50, only the ethanol monomer and water monomer and dimer are present, which are not relevant for the purpose of the present study.

In pure water clusters spectra, it was found that the main peaks are *m/z* 73 and 91, corresponding to $(H_2O)_4H^+$ and $(H_2O)_5H^+$, respectively [Figure ESM1 in Electronic Supplementary Material].

Clusters mass spectra obtained both with EI and PI for ethanol (E)-water (W) mixtures at V_E/V_S = 5% and V_E/V_S = 40% are presented in Figure 1a1-b1 and a2-b2, respectively. The spectra at an intermediate concentration (V_E/V_S = 20%) are reported in the Electronic Supplementary Material (Figure ESM2).

In Figure 1a1-b1 it is clearly shown that ethanol–water cluster molecular weights and also their signal intensities increase at higher V_E/V_S. The largest detected *m/z* value increases from ~500 at V_E/V_S = 5% to 1000 at V_E/V_S = 40%. From Figure 1a2-b2, it is evident that PI increases the signal intensity (2–3 times higher than EI) and promotes the extension of the detected clusters mass range in comparison with EI. This is in agreement with the higher expected fragmentation after electron ionization found for water clusters [31]. The comparison with pure water clusters spectra reported in a previous work [5] reveals that the clusters mass distribution is very similar only for the more diluted solution (V_E/V_S = 5%) (Figure 1a1 and a2). However, only for PI (Figure 1a2) the base peaks of the ethanol–water clusters spectra are the same with respect to pure water ones (peaks 73 and 91). In all the other spectra, included V_E/V_S = 5% with EI, the base peaks are typical of mixed ethanol–water clusters (peaks 65, 83, 93, 139), even if peaks with masses attributable to pure water clusters have comparable intensities. It means that the molecular structure of water clusters and ethanol–water clusters are similar when ethanol concentration is lower ($V_E/V_S \leq$ 5%). The presence of clusters mainly composed of the hydrogen-bonding network of water molecules, such as clusters in the pure water, was also observed by Wakisaka and Matsuura [20] for ethanol aqueous solution with low ethanol concentration (V_E/V_S < 5%).

At V_E/V_S > 5% the mass spectra are dominated by neat ethanol clusters $E_mW_nH^+$, with n = 0, mixed E–W clusters ($E_mW_nH^+$) being associated with much smaller intensities. The clusters family at fixed E and variable W are grouped in the figures, showing the main peak of each family attributable to neat ethanol clusters, starting from the dimer. It was also found the display of a magic number at $p = 21$ ($p = n + m$), in agreement with Shi et al. [32], as in the case of pure water clusters, which have enhanced abundance at the size $(H_2O)_{21}H^+$, corresponding to a clathrate structure where $(H_2O)_{20}$ forms a pentagonal dodecahedral cage with an H_3O^+ ion encaged [33]. The intensity distributions of the mixed cluster size from $n + m$ = 19 to $n + m$ = 24, with the number of ethanol molecules m in the cluster increasing from 3 to 5, are

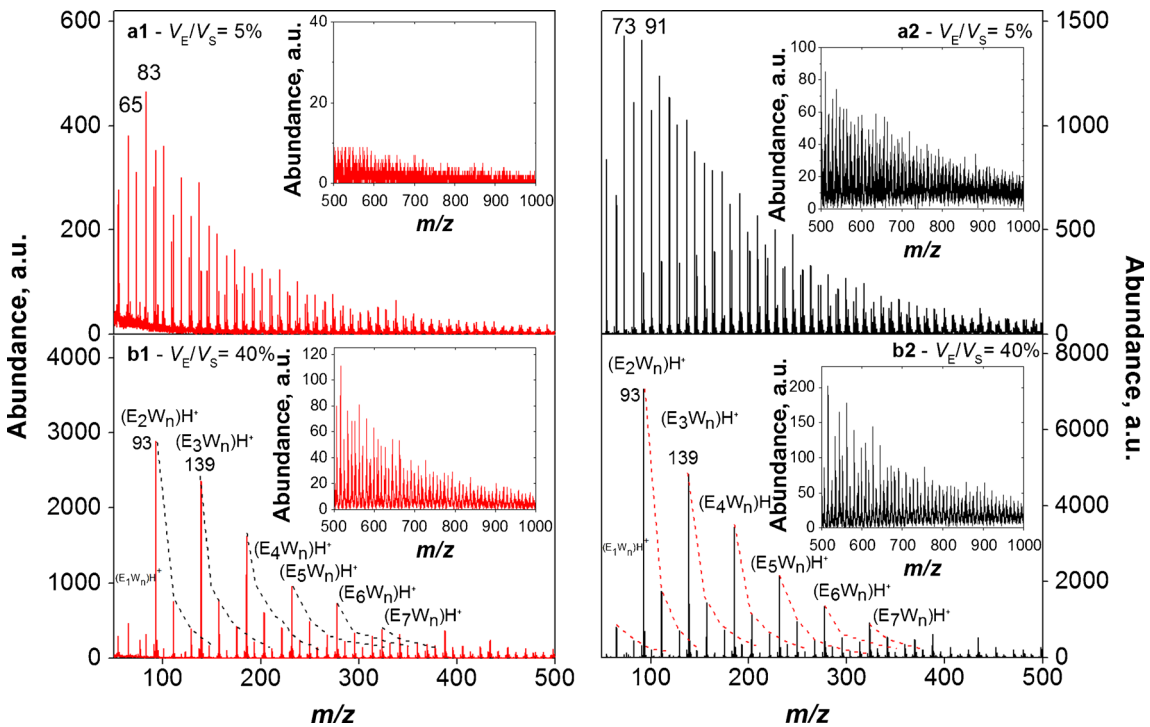

Figure 1. Mass spectra of water clusters with different ethanol/solution ratios with EI: **(a1)** 5% V_E/V_S, **(b1)** 40% V_E/V_S, and with laser PI: **(a2)** 5% V_E/V_S, **(b2)** 40% V_E/V_S. In **b1**-**b2**, ethanol water clusters [$(E_mW_n)H^+$] series are grouped. The m = 1 series is characterized by $n \geq 1$ (the pure ethanol, i.e.. the monomer, is not reported). For the $m \geq 2$ series n is ≥ 0 (pure ethanol clusters are present too)

reported in the Electronic Supplementary Material (Figure ESM 3).

The changes into composition distribution of ethanol–water clusters at higher ethanol volumetric ratios with EI and PI are better observable in Figure 2. In this figure, the composition distribution of $E_mW_nH^+$ cluster is sketched in a tridimensional graph, by reporting the abundance of detected cluster ions as a function of the number m (0–24) of ethanol molecules and of the number n (0–24) of water molecules in each cluster.

The composition distributions of ethanol–water clusters with EI and PI at V_E/V_S = 5% and 40%, are shown in Figures 2a1-b1 and 2a2-b2, respectively. The distributions at an intermediate concentration (V_E/V_S = 20%) are reported in the Electronic Supplementary Material (Figure ESM 4).

It is clearly shown that by increasing the ethanol concentration from 5% up to 40%, the spectral pattern gradually changes and water-rich clusters signals become fainter while ethanol-rich clusters signals become more intense.

In Figure 2a1-a2 (at V_E/V_S = 5%) it is possible to observe that the mass distribution remains very similar to the pure water (m = 0) also in the case of m = 1–3, especially in the case of PI (Figure 2a2), where also the base peaks are the same (i.e., m/z 73 and 91, corresponding to W_4H^+ and W_5H^+). The maximum number of water molecules in the clusters reaches up to n = 24. In the case of EI, the base peaks are already shifted to m/z 65 and 83, corresponding to $E_1W_1H^+$ and $E_1W_2H^+$. However, both spectra indicate that at V_E/V_S = 5% the microscopic structures of clusters are mainly composed of the hydrogen-bonding network of water molecules, in agreement with Wakisaka [20].

As V_E/V_S increases to 40% (Figure 2b1-b2), the distributions appear different, with the maximum number of water molecules in the clusters of each series decreasing up to 4–6 and, in the meantime, the based peak shifting from m/z 65 and 83 [corresponding to the cluster ions of 1–1 and 1–2 ($m-n$, $E_1W_1H^+$) and $E_1W_2H^+$)] to m/z 93 and 139 [corresponding to the cluster ions of 2–0 and 3–0 ($m-n$, E_2H^+ and E_3H^+)]. In other words, there is a shift from water-rich clusters to ethanol-rich clusters with the increase of the ethanol concentration.

The large hydrogen-bonding network of pure water progressively changes in order to coexist with ethanol self-association clusters. Moreover, at V_E/V_S = 40% the highest signals are presented by clusters with $n < 4$ and $m < 8$ but it is noteworthy to observe that big ethanol clusters with m up to 20–24 are formed. As in the literature Wakisaka [20] reported the formation in pure ethanol of clusters just up to m = 4, the role of water in promoting the self-association of ethanol with a process called "complementary relationship" [20] can be claimed on the basis of our results. Moreover, at higher ethanol concentrations the formation of hydrated clusters with high value of m and n was found not favored. These findings are in agreement with the hypothesis first proposed by Nishi et al. [14, 15] that

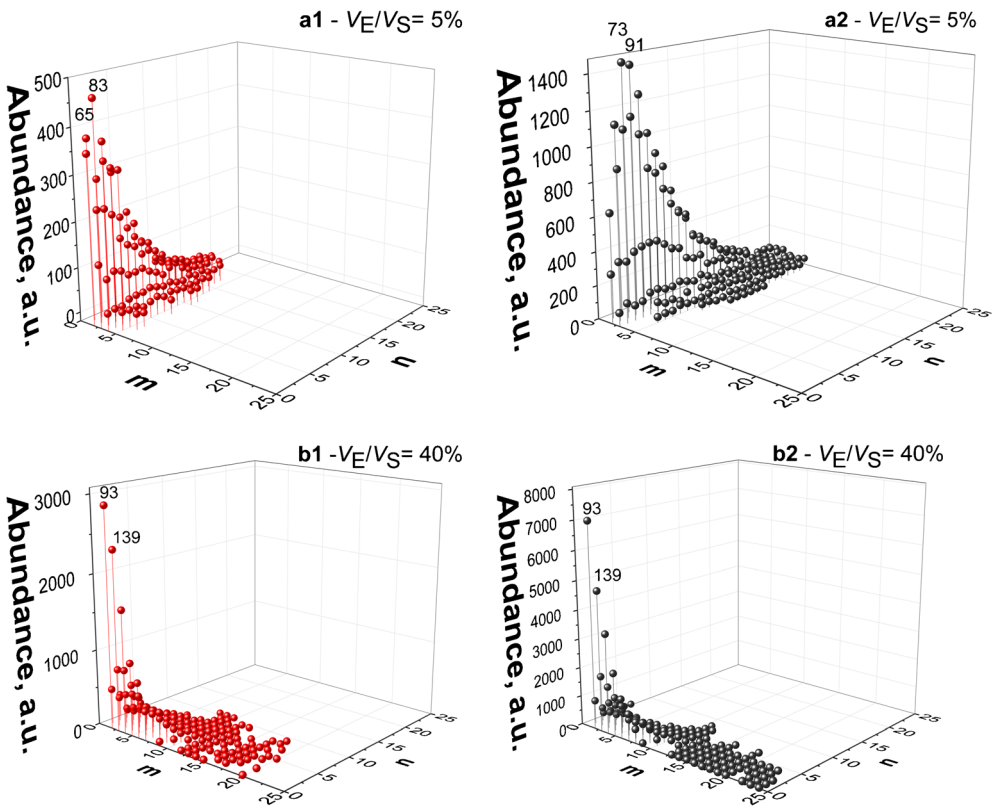

Figure 2. Composition distribution of ethanol-water clusters, in terms of the number of water molecules (n) and ethanol molecules (m) determined in each cluster, at different ethanol/solution ratios with EI: **(a1)** 5% V_E/V_S; **(b1)** 40% V_E/V_S and with laser PI: **(a2)** 5% V_E/V_S ; **(b2)** 40% V_E/V_S

the formation of higher hydrates is endothermic in contrast to the exothermic ethanol association processes in ethanol–water binary mixtures by ethanol–water cluster evolution-dissociation equilibrium calculations. Nishi et al. [14] also reported that the hydrogen bonds between less mobile molecules (ethanol with respect to water due to its higher MW) can be formed for a longer time than those of small molecules, so in the ethanol aqueous binary mixture, the EtOH–EtOH interactions are more stable than those of EtOH–H_2O and H_2O–H_2O. This is probably due to the fact that the water attachment involves the breaking of an ethanol–ethanol bond, which is highly stabilized in the aqueous system. At V_E/V_S > 20% the hydrogen bonding between water molecules becomes very weak compared with the ethanol–ethanol bond.

The magic number at $p = 21$ was not displayed by clusters at such high ethanol concentrations.

Owing to the high ionization efficiency of laser at 355 nm, much more intense clusters peak signals and larger MW range are observed at any V_E/V_S value with PI compared with EI. In order to quantitatively compare the effect of different ionization methods, the parameter $I_{200\sim1000}/I_{50\sim200}$ was used, where $I_{50\sim200}$ and $I_{200\sim1000}$ represent the sum of peak intensities of clusters in the *m/z* range of 50~200 and 200~1000 at the same ethanol solution concentration, respectively.

$I_{200\sim1000}/I_{50\sim200}$ with EI is in the range of 0.45~1.27, whereas $I_{200\sim1000}/I_{50\sim200}$ with laser ionization is in the range of 2.28~2.59. This quantitatively shows that clusters mass range is smaller with EI in comparison with laser photo-ionization. This is due to a larger fragmentation occurring in the ionization region when a hard ionization system such EI at 70 eV is employed.

In the present work, the following characteristics for ethanol–water binary mixtures have been inferred on the basis of the observations from mass spectra with both ionization systems: (1) the water clusters molecular structures based on the hydrogen-bonding network remain initially intact with ethanol addition, with just the progressive substitution of some water molecules with ethanol molecules. When V_E/V_S becomes ≥20% the network is disrupted with the formation of ethanol–ethanol clusters; (2) microscopic phase separation at the cluster level takes place in ethanol–water binary mixtures; (3) the increase of ethanol concentration promotes the formation of hydrated ethanol clusters and the self-association of ethanol clusters becomes dominant in ethanol–water binary mixtures.

With an increase of the ethanol concentration to 40%, the signal intensity of mass distribution series with $n = 0$ (E_mH^+, ethanol clusters) significantly increases; in the meantime, more series m = 12–24 appear, whereas the maximum number of water molecules in the clusters of each series decreases to 4–6 compared with 14 at V_E/V_S = 20% and 24 at V_E/V_S = 5%. This result is in agreement with Coccia et al. [34] findings about the study on the chemical shifts of the hydroxyl signal in water–ethanol mixtures with high resolution nuclear magnetic resonance spectroscopy, which showed that the hydrogen-bonding lifetimes of water were much shorter at high ethanol concentration.

Autocorrelation Analysis of the Clusters Mass Spectra

In the present work, the autocorrelation function (AF) has been used to analyze the composition of the ethanol and water clusters in terms of periodicities. The application of AF to mass spectra analysis has been reported in details in a previous paper [35], where its advantages in water clusters spectra analysis are shown with respect to other approaches. Briefly, AF can be defined as:

$$y(\tau) = \sum_{0}^{M-1} f(t)f(t-\tau)$$

where *f(t)* represents a discrete signal of the length *M*, and *f(t- τ)* represents the "delayed" version of *f(t)* by the interval *τ*. The magnitude of the computed correlation shows the degree of self-similarity of the signals as a function of the delay. If the magnitude of the autocorrelation function is large, the delayed signal should be considered very similar to the original one. Alternatively, if it is close to zero, the signal is considered not to keep the same relation between two points as the delay increases.

The autocorrelation of ethanol–water clusters spectra at V_E/V_S = 5% with electron ionization from *m/z* 50 to 500 is reported in Figure 3a1-b1; the results are normalized and the magnitude ranges from 0 to 1. The spectra at V_E/V_S = 20% are reported in the Electronic Supplementary Material (Figure ESM5).

As shown in Figure 3a1, several significantly high correlations (normalized AF > 0.5) can be observed, corresponding to *m/z* intervals of 10, 18, 28, 36, 46, 54, and 64. The notable peak is at an interval of *m/z* 18, with its multiples at *m/z* 36, 54, 72, which correspond to single water molecule additions, whereas the peak at *m/z* 10 corresponds to the mass difference between the clusters $E_mW_{n-1}H^+$ and $E_{m-1}W_{n+1}H^+$ and *m/z* 28 peak represents the mass difference between the clusters $E_mW_{n-1}H^+$ and $E_{m-1}W_nH^+$. Another notable peak is at *m/z* 46, which represents the addition of an ethanol molecule.

With the increase of V_E/V_S ratio from 5% to 40%, the autocorrelation function value for *m/z* 18 and its multiples decreases, and AF for the peak of *m/z* 46 and its multiples increases. It is noticeable that at V_E/V_S = 20% (Figure ESM 5) and 40% (Figure 2b1), the *m/z* 18 peak and its multiples are not significant, whereas the *m/z* 46 peak is significant and even the significant *m/z* 92 peak appears at V_E/V_S = 40%. Through the analysis of AF, it is easy to obtain the information on the composition of the clusters: the correlation of *m/z* 18 and its multiples at V_E/V_S = 5% indicates the mass spectrum is dominated by water-rich clusters, whereas the correlation of *m/z* 46 and its multiples at V_E/V_S = 20% and 40% indicates that the mass spectrum is dominated by ethanol-rich clusters. Similar results were observed for ethanol–water clusters with PI (Figure 3a2-b2, Figure ESM5).

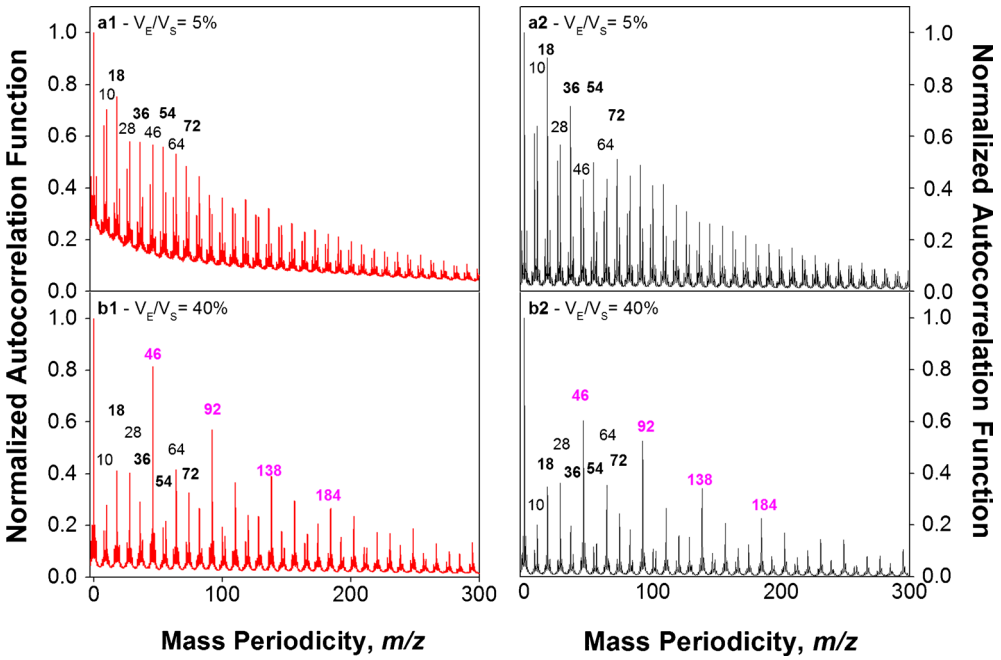

Figure 3. Autocorrelation of water clusters spectra with different ethanol/solution ratios with EI: **(a1)** 5% V_E/V_S; **(b1)** 40% V_E/V_S and with laser PI: **(a2)** 5% V_E/V_S ; **(b2)** 40% V_E/V_S. Labels for mixed ethanol-water (black), pure water (black, bolded) and pure ethanol (magenta, bolded) clusters are reported too

These findings demonstrate the utility of using AF analysis for a rapid screening of the spectra, especially useful when many spectra (for example at different concentrations) are to be managed.

Cluster Composition Distribution: Molar Ratio of Ethanol to Water in the Observed Clusters (R_E)

The sum of peak intensities of cluster ions containing m molecules of ethanol fragments is calculated as ΣI_m (I being the peak intensity). The sum (ΣI_m) multiplied by the number m, which is $m\Sigma I_m$, is then proportional to the total number of ethanol fragment molecules in the cluster ions containing m molecules of ethanol fragments. The sum (Σ_E) of $m\Sigma I_m$ calculated from the whole mass spectrum is also assumed to be proportional to the total number of ethanol fragment molecules in all cluster ions.

In the same way, indicating with I_n the peak intensity of cluster ions containing n molecules of water, the sum (Σ_W) of $n\Sigma I_n$ calculated from the whole mass spectrum can be assumed to be proportional to the total number of water molecules in all ions. Thus, the intensity ratio of ethanol to water in the observed clusters, R_E value, can be calculated as: Σ_E/Σ_W. The procedure is very similar to that reported by Tsuchiya et al. [36] to calculate the ethanol/water molar ratio in gas phase.

Figure 4 reports the intensity ratio (R_E) for ethanol–water clusters acquired with EI and PI at different composition of ethanol/water mixtures to quantitatively compare the different ionization methods performances. R_E shows an increase with both ionization methods by increasing ethanol–solution volume ratio in a concentration range 0%–40%. In agreement with the achievements from Figure 2, the ethanol-rich clusters intensities increase with increasing ethanol concentrations, and this trend is a bit more accentuated with PI, especially after 10% of V_E/V_S ratio. The ethanol concentration in the observed clusters is found to be much higher than that in the sample solution (ethanol mole fraction x_E, also reported in the figure).

This feature indicates the micro-heterogeneity of the ethanol–water binary mixture, which is composed both of ethanol-rich and water-rich clusters, with weak interactions between them. In other words, ethanol–water solutions show incomplete mixing at the molecular level, as already reported in the literature in similar solution concentration ranges [16, 20, 21].

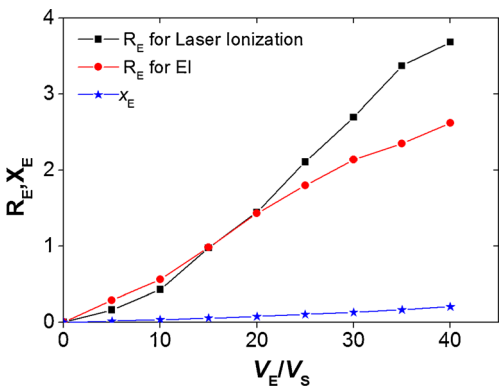

Figure 4. Comparison between the intensity ratio (R_E, see text for definition), obtained for EI and PI and ethanol mole fractions in the liquid solution (x_E) at different V_E/V_S ratios. Errors are estimated to be about 10% for all R_E values and therefore not reported

Table 2. y_E Evaluated for Different Experimental Methods: Neutron Diffraction [17], Linear TOFMS (*l*–TOFMS) [18], and Reflectron TOFMS (*r*–TOFMS) with EI and PI Sources [Present Study]

x_E	y_E			
	Neutron diffraction[a] (error not reported)	l–TOFMS with nanosecond PI[b] (error ±0.02)	EI r–TOFMS[c] (error ±10%)	PI r–TOFMS[c] (error ±10%)
0.022	0.12	0.14	0.33	0.19
0.045	0.21	0.25	0.46	0.44
0.1	0.34	0.45	0.63	0.68
0.24	0.62	0.72	0.79	0.84

[a]Reference [17].
[b]Reference [18].
[c]Present study.

The ethanol molar fractions in gas phase, y_E, evaluated from different methods reported in literature, are listed in Table 2 along with those obtained from the present study (calculated as $\Sigma_E/(\Sigma_E+\Sigma_W)$). From Table 2 it can be observed that mass spectrometry (reported in present and previous studies [20, 21]) gives higher y_E values with respect to neutron reflection ones, probably due to the contrast in scattering of the surface layer and the bulk when neutron reflection is employed.

The y_E values obtained with our method are larger than that obtained from linear TOFMS (*l*–TOFMS) with nanosecond laser photo-ionization at the same solution condition [18], especially at higher concentrations. This is because much larger ethanol-rich clusters were detected in our experiments. For example, the bigger clusters detected by our mass spectrometer with EI and PI are $E_{17}W_6H^+$ and $E_{24}W_7H^+$ at $x_E = 0.1$, respectively, whereas the bigger clusters detected by Raina et al. [18] were only $E_4W_1H^+$ at the same x_E value .

It is interesting to note from Figure 4 that for V_E/V_S higher than 20%, also the slope of the intensity ratio ethanol to water in the vapor phase, R_E, changes and its values tend to decrease, showing a sort of saturation, for EI. This noteworthy finding can be interpreted with the decreasing of ethanol-richer clusters intensity with respect to ethanol hydrated clusters in more

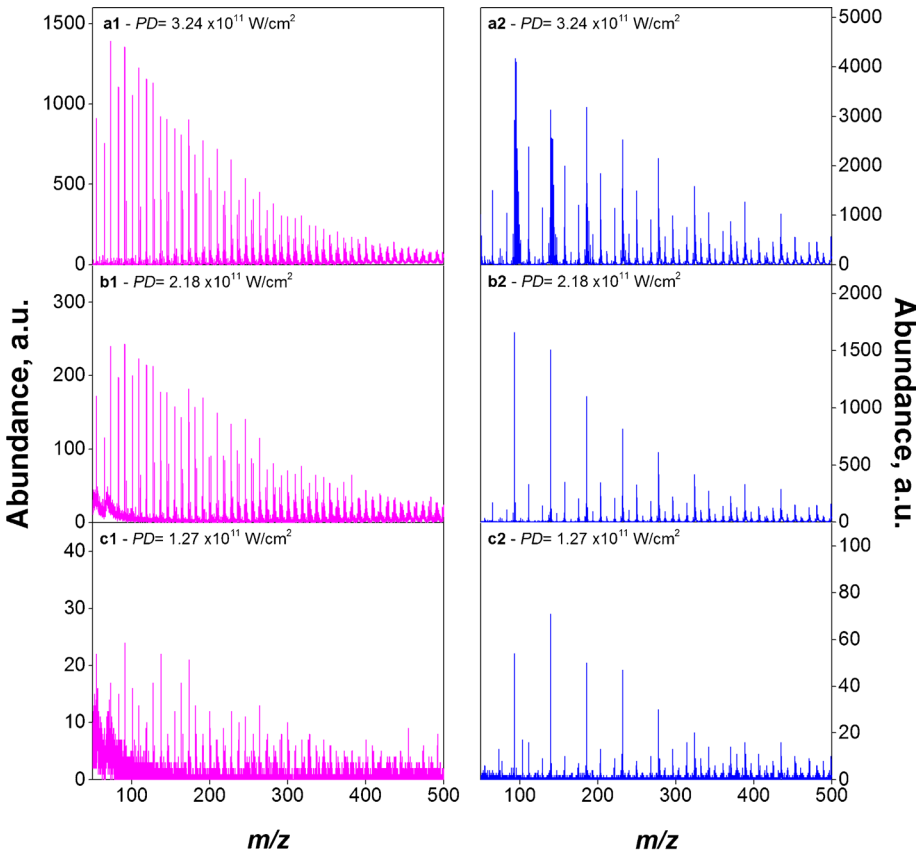

Figure 5. Mass spectra of clusters for the ethanol–water solutions at $V_E/V_S = 5\%$ (series 1) and $V_E/V_S = 40\%$ (series 2) with *PD* 3.24 **(a1**, **a2)**; 2.18 **(b1**, **b2)**; 1.27 **(c1**, **c2)** $\times 10^{11}$ W/cm^2

concentrated solutions, suggesting a role of water in promoting ethanol self-association.

The finding observed by EI is probably due to the fact that the richer ethanol clusters are more prone to fragmentation at hard ionization conditions with respect to ethanol–hydrated clusters, confirming the previous observation about the hydrogen-bond network disruption when the ethanol concentration is higher than 20%.

Dependence of Cluster Mass Spectra on Laser Power Density (PD)

The mass spectra of clusters for the ethanol–water binary mixture solutions at V_E/V_S = 5% and 40% obtained with different laser *PD* are shown in Figure 5. Both at V_E/V_S = 5% and 40%, it is clearly shown that the signal intensity sharply decreases with a decrease in the *PD* of 30% with respect to the maximum laser pulse energy (Figure 5b1-b2) and only weak signals appear with a laser power density decrease of 60% (Figure 5c1-c2).

The metastable fragment cluster ions, created in the field-free region of TOFMS, can be easily discriminated in the reflectron section of the TOF mass spectrometer since they appear as satellites to the main unfragmented protonated cluster ion peaks [24]. In order to confirm the identification of those peaks as metastable peaks, the potentials of the reflector were varied systematically. It has been observed that the features of each set of parent–daughter peaks (i.e. the height, the position, and the width of the peaks), are influenced by the potentials of the reflector much more than features of parent ions pairs, confirming their identification as metastable peaks [37]. Therefore, $E_IW_nH^+$ parent and metastable fragment cluster distributions of ethanol–water binary mixture solution at V_E/V_S = 5% for several values of the laser power density have been identified and reported in Figure 6. It is remarkable that the maximum intensity of parent clusters peak occurs at n = 2–5, whereas the maximum of metastable fragments clusters peak is at n = 12–15 because the metastable fragmentation rate of small clusters is very low. The parent clusters intensities are much higher than those of metastable fragments for small clusters ($n < 21$), whereas the signal intensity shows no significant differences between parent and metastable fragments for larger clusters ($n \geq 21$). The parent and metastable fragments clusters distributions obtained with laser ionization are similar

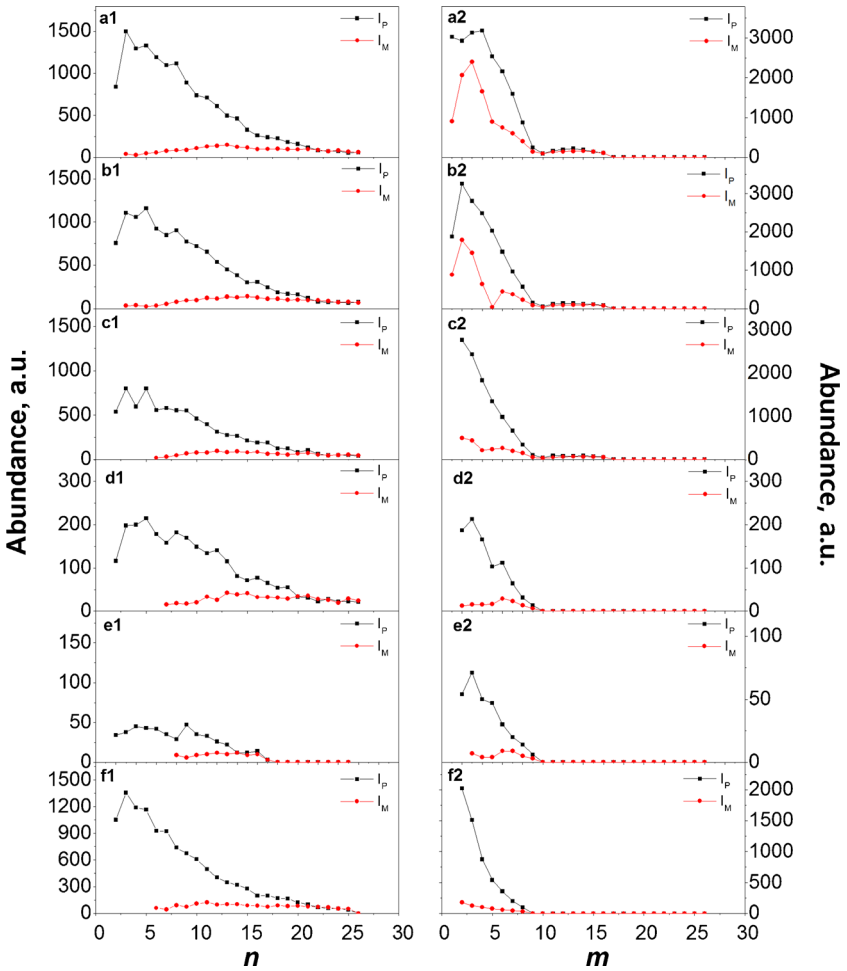

Figure 6. Metastable fragmentation of the $E_IW_nH^+$ cluster at V_E/V_S = 5% (series 1) and E_mH^+ cluster at V_E/V_S = 40% (series 2) with *PD* 3.24 **(a1, a2)**; 2.81 **(b1, b2)**; 2.53 **(c1, c2)**; 2.18 **(d1, d2)**; 1.62 **(e1, e2)** $\times 10^{11}$ W/cm^2, and EI **(f1, f2)**

to those obtained by using electron ionization as shown in Figure 6 f1, in agreement with the findings reported on pure water clusters by using photoionization [5, 27, 29] and chemical ionization [38]. Indeed, in a previous paper [5] it was found that the pure water clusters spectrum is composed of two sequences: a main sequence, corresponding to parent peaks of water clusters W_nH^+, with decreasing intensity as MW increases, and a second sequence, corresponding to metastable peaks, with intensity much lower for small clusters, increasing with MW up to being comparable to the main one at *m/z* around 400 (corresponding to clusters with $n = 21$, as found in the present study).

The obtained results suggest that the formation of water-rich clusters and subsequent metastable fragmentation is the dominant process that determines the cluster distribution, irrespective of the initial ionization process. They also suggest that the $E_1W_nH^+$ cluster distributions of the ethanol water binary mixture solution with low ethanol concentration ($V_E/V_S = 5\%$) show similar characteristics with respect to the water cluster.

The mass spectra are dominated by the ethanol-rich clusters at $V_E/V_S = 40\%$; therefore, in Figure 6 the E_mH^+ parent and metastable fragment cluster distributions of ethanol–water binary mixture solution at $V_E/V_S = 40\%$ as a function of the laser power density are also presented. The maximum intensity of parent clusters peak is observable at $n = 2$–4 in all the *PD* ranges. The metastable fragment clusters intensity is similar to the parent peak intensity at high laser power density ($PD = 3.24 \times 10^{11}$ W/cm^2 and 2.81×10^{11} W/cm^2) (Figure 6a2-b2), whereas it is much lower for small clusters ($m < 9$) at low laser power densities (i.e., $PD \leq 2.53 \times 10^{11}$ W/cm^2) and by using EI (Figure 6c2-f2). This suggests that the ionization process significantly affects the ethanol-rich cluster distribution, which is different from the water-rich clusters.

In order to compare the change of mass spectra range by changing the laser *PD*, the parameter $I_{200\sim1000}/I_{50\sim200}$ at $V_E/V_S = 5\%$ and 40% with different laser power densities was calculated, where $I_{200\sim1000}$ is the sum of the intensities of peaks in the MW range 200–1000 Da, whereas $I_{50\sim200}$ is the sum of the intensities of peaks in the MW range 50–200 Da, as introduced in the previous paragraphs. $I_{200\sim1000}/I_{50\sim200}$ ratio significantly decreases with increasing the *PD* for both the V_E/V_S values (Figure ESM 6 in Electronic Supplementary Material), which suggests that the smaller molecular masses dominate the spectra with increasing laser power density at every ethanol concentration. This could be due merely to a larger fragmentation occurring in the ionization region with increasing laser power density. As expected, it is found that the lower $I_{200\sim1000}/I_{50\sim200}$ ratio value and, therefore, the higher fragmentation, is produced by using EI, even in comparison with the maximum *PD* (Figure ESM 6 in Electronic Supplementary Material).

A further explanation could be the occurrence of a different order of multiphoton ionization processes for small and big clusters, as previously found for pure water clusters [5]. A slope change of the intensity of the ion signal versus *PD* was found for pure water clusters just in correspondence of $n = 10$ (MW about 200 Da). In particular, for water clusters containing more than 10 molecules, the slope is around three (3.3 ± 0.3), indicating that a three-photon ionization process takes place. By contrast, for water clusters smaller than 10 molecules, the slope is around four (4.5 ± 0.3) [5]. This occurrence could justify such a rapid decreasing of $I_{200\sim1000}/I_{50\sim200}$ ratio with increase in the power density. However, more study is necessary in order to confirm this hypothesis.

Conclusions

In this paper, clusters molecular mass distributions of pure water and ethanol aqueous solutions were obtained by using a Reflectron TOFMS (*r*–TOFMS) apparatus with two different ionization sources: EI and PI (at 355 nm).

PI has been shown to increase the signal intensity and enlarge the detection mass range of the clusters in comparison with EI. Smaller molecular masses with EI arose in comparison with laser ionization, which has been related to a larger fragmentation occurring in the ionization region when a hard ionization system such as EI is employed. Much larger clusters were detected in our experiments with respect to the current literature.

It was demonstrated that the autocorrelation function (AF) is an efficient method for analyzing the composition of the water/ethanol clusters in terms of fundamental periodicities. It gives the possibility of a rapid screening of the spectra to follow the change in clusters distribution while changing the ethanol concentration in solution.

It was found that the water cluster structures based on the hydrogen-bonding network are disrupted with the addition of ethanol, and ethanol molecules are capable of substitutional interaction with hydrogen-bonded water clusters in ethanol–water binary mixtures. Self-association of ethanol is dominant, and the increase of ethanol concentration promotes the formation of hydrated ethanol clusters and the self-association of ethanol clusters in ethanol–water binary mixtures.

The formation of water-rich clusters and subsequent metastable fragmentation is the dominant process that determinates the clusters distribution, irrespective of the initial ionization process, whereas the initial ionization process significantly affects the ethanol-rich clusters distribution.

Acknowledgments

The authors thank the MSE-CNR project on Carbone Pulito for financial support.

References

1. Torchet, G., Schwartz, P., Farges, J., Feraudy, M.F., Raoult, B.: Structure of solid water clusters formed in a free jet expansion. J. Chem. Phys. **79**, 6196–6202 (1983)
2. Beuhler, R.J.: Electron-impact ionization of negatively charged water-cluster ions. Phys. Rev. Lett. **58**, 13–16 (1987)

3. Adoui, L., Cassimi, A., Gervais, B., Grandin, J.-P., Guillaume, L., Maisonny, R., Legendre, S., Tarisien, M., López-Tarifa, P., Politis, M.-F., Hervé du Penhoat, M.-A., Vuilleumier, R., Gaigeot, M.-P., Tavernelli, I., Alcamí, M., Martín, F.: Ionization and fragmentation of water clusters by fast highly charged ions. J. Phys. B: At. Mol. Opt. Phys. **42**, 075101–075106 (2009)
4. Mizuse, K., Mikami, N., Fujii, A.: Infrared spectra and hydrogen-bonded network structures of large protonated water clusters H+(H2O)n (n = 20–200). Angew. Chem. Int. Ed. **49**, 10119–10122 (2010)
5. Apicella, B., Li, X., Passaro, M., Spinelli, N., Wang, X.: Multiphoton ionization of large water clusters. J. Chem. Phys. **140**, 204313–204318 (2014)
6. Mizuse, K.: Spectroscopic investigations of hydrogen bond network structures in water clusters, pp. 1–12. Springer, Japan (2013)
7. Mizuse, K., Kuo, J.-L., Fujii, A.: Structural trends of ionized water networks: infrared spectroscopy of water cluster radical cations $(H_2O)_n^+$ (n = 3–11). Chem. Sci. **2**, 868–876 (2011)
8. Mizuse, K., Fujii, A.: Characterization of a solvent-separated ion-radical pair in cationized water networks: infrared photodissociation and Ar attachment experiments for water cluster radical cations $(H_2O)_n^+$ (n = 3–8). J. Phys. Chem. A **117**, 929–938 (2013)
9. Golan, A., Ahmed, M.: Ionization of water clusters mediated by excit on energy transfer from argon clusters. J. Phys. Chem. Lett. **3**, 458–462 (2012)
10. Bing, D., Hamashima, T., Fujii, A., Kuo, J.L.: Anticooperative effect induced by mixed solvation in $H^+(CH_3OH)_m(H_2O)_n$ ($m + n$ = 5 and 6): a theoretical and infrared spectroscopic study. J. Phys. Chem. A **114**, 8170–8177 (2010)
11. Franks, F., Ives, D.J.G.: The structural properties of alcohol–water mixtures. Q. Rev. Chem. Soc. **20**, 1–44 (1966)
12. Schofield, R.K., Rideal, E.K.: Kinetic theory of surface films. Parts I and II. Proc. Roy. Soc. Lond. A **109**, 57–77 (1925)
13. Matsumoto, M., Nishi, N., Furusawa, T., Saita, M., Takamuku, T., Yamagami, M., Yamaguchi, T.: Structure of clusters in ethanol–water binary solutions studied by mass spectrometry and X-Ray diffraction. Bull. Chem. Soc. Jpn. **68**, 1775–1783 (1995)
14. Nishi, N., Koga, K., Ohshima, C., Yamamoto, K., Nagashima, U., Nagami, K.: Molecular association in ethanol–water mixtures studied by mass spectrometric analysis of clusters generated through adiabatic expansion of liquid jets. J. Am. Chem. Soc. **110**, 5246–5255 (1988)
15. Nishi, N., Takahashi, S., Matsumoto, M., Tanaka, A., Muraya, K., Takamuku, T., Yamaguchi, T.: Hydrogen-bonded cluster formation and hydrophobic solute association in aqueous solutions of ethanol. J. Phys. Chem. **99**, 462–468 (1995)
16. Egashira, K., Nishi, N.: Low-frequency Raman spectroscopy of ethanol−water binary solution: evidence for self-association of solute and solvent molecules. J. Phys. Chem. B **102**, 4054–4057 (1998)
17. Li, Z.X., Lu, J.R., Styrkas, D.A., Thomas, R.K., Rennie, A.R., Penfold, J.: The structure of the surface of ethanol/water mixtures. Mol. Phys. **80**, 925–939 (1993)
18. Raina, G., Kulkarni, U., Rao, C.N.R.: Mass spectrometric determination of the surface compositions of ethanol–water mixtures. Int. J. Mass Spectrom. **212**, 267–271 (2001)
19. Raina, G., Kulkarni, U., Rao, C.N.R.: Surface enrichment in alcohol−water mixtures. J. Phys. Chem. A **105**, 10204–10207 (2001)
20. Wakisaka, A., Matsuura, K.: Microheterogeneity of ethanol−water binary mixtures observed at the cluster level. J. Mol. Liq. **129**, 25–32 (2006)
21. Wakisaka, A., Ohki, T.: Phase separation of water–alcohol binary mixtures induced by the microheterogeneity. Faraday Discuss. **129**, 231–245 (2005)
22. Kostko, O., Belau, L., Wilson, K.R., Ahmed, M.: Vacuum-ultraviolet (VUV) photoionization of small methanol and methanol–water clusters. J. Phys. Chem. A **112**, 9555–9562 (2008)
23. Kusalik, P.G., Lynbartsev, A.P., Bergman, D.L., Laaksonen, A.: Computer simulation study of tert-butyl alcohol. 1. Structure in the pure liquid. J. Phys. Chem. B **104**, 9526–9532 (2000)
24. Ebata, T., Fujii, A., Mikami, N.: Vibrational spectroscopy of small-sized hydrogen-bonded clusters and their ions. Int. Rev. Phys. Chem. **17**, 331–361 (1998)
25. Wu, C.-C., Chaudhuri, C., Jiang, J.C., Lee, Y.T., Chang, H.-C.: Structural isomerism and competitive proton solvation between methanol and water in $H^+(CH_3OH)_m(H_2O)_n$, $m + n = 4$. J. Phys. Chem. A **108**, 2859–2866 (2004)
26. Belau, L., Wilson, K.R., Leone, S.R., Ahmed, M.: Vacuum ultraviolet (VUV) photoionization of small water clusters. J. Phys. Chem. A **111**, 10075–10083 (2007)
27. Radi, P.P., Beaud, P., Franzke, D., Frey, H.-M., Gerber, T., Mischler, B., Tzannis, A.-P.: Femtosecond photoionization of $(H_2O)_n$ and $(D_2O)_n$ clusters. J. Chem. Phys. **111**, 512–518 (1999)
28. Panariello, M., Apicella, B., Armenante, M., Bruno, A., Ciajolo, A., Spinelli, N.: Analysis of polycyclic aromatic hydrocarbon sequences in a premixed laminar flame by on-line time-of-flight mass spectrometry. Rapid Commun. Mass Spectrom. **22**, 573–581 (2008)
29. Apicella, B., Wang, X., Armenante, M., Bruno, A., Spinelli, N.: Picosecond and nanosecond laser ionization for the on-line analysis of combustion-formed pollutant. Proceedings of the 32nd Meeting of the Italian Section of Combustion Institute, Naples, Italy, April 26–28 (2009). http://www.combustion-institute.it/proceedings/proc2009/data/I/I-12.pdf. Accessed 29 June 2015
30. Stace, A.J., Shukla, A.K.: Preferential solvation of hydrogen ions in mixed clusters of water with methanol and ethanol. J. Am. Chem. Soc. **104**, 5314–5318 (1982)
31. Lengyel, J., Pysanenko, A., Poterya, V., Kočišek, J., Fárník, M.: Extensive water cluster fragmentation after low energy electron ionization. Chem. Phys. Lett. **612**, 256–261 (2014)
32. Shi, Z., Wei, S., Ford, J.V., Castleman, A.W.: Clathrate structures in water–methanol mixed clusters. Chem. Phys. Lett. **200**, 142–146 (1992)
33. Wei, S., Shi, Z., Castleman, A.W.: Mixed cluster ions as a structure probe: experimental evidence for clathrate structure of $(H_2O)_{20}H^+$ and $(H_2O)_{21}H^+$. J. Chem. Phys. **94**, 3268–3270 (1991)
34. Coccia, A., Indovina, P.L., Podo, F., Viti, V.: PMR Studies on the structures of water–ethyl alcohol mixtures. Chem. Phys. **7**, 30–40 (1975)
35. Apicella, B., Bruno, A., Wang, X., Spinelli, N.: Fast Fourier transform and autocorrelation function for the analysis of complex mass spectra. Int. J. Mass Spectrom. **338**, 30–38 (2013)
36. Tsuchiya, M., Shida, Y., Kobayashi, K., Taniguchi, O., Okouchi, S.: Cluster composition distribution at the liquid surface of alcohol–water mixtures and evaporation processes studied by liquid ionization mass spectrometry. Int. J. Mass Spectrom. **235**, 229–241 (2004)
37. Wei, S.Q., Castleman, A.W.: Using reflection time-of-flight mass spectrometer techniques to investigate cluster dynamics and bonding. Int. J. Mass Spectrom. Ion Processes **131**, 233–264 (1994)
38. Crowell, R.A., Bartels, D.M.: Multiphoton ionization of liquid water with 3.0−5.0 eV photons. J. Phys. Chem. **100**, 17940–17949 (1996)